applied sciences

MDPI

Article

Examination of Couette Flow with a Pressure Gradient and Heat Conduction Using Molecular Dynamics Simulation

Esma Pala Öngül [1,*] and İlyas Kandemir [2]

[1] Mechanical Engineering Department, Gebze Technical University, Kocaeli 41400, Türkiye
[2] Aeronautical Engineering Department, Gebze Technical University, Kocaeli 41400, Türkiye; kandemir@gtu.edu.tr
* Correspondence: esma.pala@gtu.edu.tr

Featured Application: This study aims to fill a knowledge gap in rarefied gas flows, addressing the complexities related to wall temperatures and pressure differentials in the simulation of gas–solid interactions in nanoscale and microscale geometries. The findings are relevant to diverse microfluidic applications, encompassing devices such as micro–nano electronic devices. Simulations were carried out in non-dimensional form so that the results can be extended to all noble gases.

Abstract: As computer capabilities improve, Molecular Dynamics simulations are becoming more important for solving various flow problems. In this study, Couette and Poiseuille flows at different wall temperatures were investigated using a hard-sphere Molecular Dynamics simulation approach. Although a low spacing ratio was used in the simulations, the results are valid for rarefied gas flows when proper scaling based on the Knudsen number was used because only binary collisions with a hard-sphere model were considered. The main focus of this study was the examination of the effects of various wall speeds, pressure gradients, and wall temperatures. A pressure gradient was generated by developing a modified selective periodicity condition in the flow direction. With the combined effect of the pressure gradient and the wall velocities, subsonic, transonic, and supersonic speeds in nanochannels were examined. With the combination of different parameters, 1260 simulation cases were conducted. The results showed that there are temperature and velocity slips that are dependent on not only the temperature and velocity values but also on the magnitudes of a pressure gradient. The pressure gradient also caused nonlinearities in temperature and velocity profiles.

Keywords: molecular dynamics; simulation; hard-sphere; Couette flow; pressure gradient

Citation: Pala Öngül, E.; Kandemir, İ. Examination of Couette Flow with a Pressure Gradient and Heat Conduction Using Molecular Dynamics Simulation. *Appl. Sci.* **2024**, *14*, 2313. https://doi.org/10.3390/app14062313

Academic Editor: Francesca Scargiali

Received: 7 February 2024
Revised: 2 March 2024
Accepted: 4 March 2024
Published: 9 March 2024

1. Introduction

Molecular dynamics (MD) simulations are widely used in various scientific and engineering fields due to their ability to provide insights into the behavior and interactions of molecules and materials at the atomic and molecular levels. Recently, there have been notable advancements in micro- and nanoelectromechanical systems (MEMS, NEMS), resulting in the creation of diverse applications [1]. Therefore, the examination of gas flows in micro- and nanochannels has become crucial for the development and functioning of microdevices like microvalves, micropumps, and microturbines. This research study emphasizes the significance of examining gas flows in these microchannels and their impact on industrial applications. This study investigates Couette and Poiseuille flows combined using a hard-sphere MD simulation approach. The results show that temperature and velocity slips depend on wall speeds, pressure gradients, and wall temperatures, causing nonlinearities. Since many numerical methods fail to adequately represent nanochannel flows and experimental studies are also very difficult, MD simulations have become very important.

When it comes to the theoretical foundation for comprehending the actions of gases on a molecular scale, the kinetic theory of gases is a fundamental principle in physics. This theory considers gases to be ensembles of particles [2,3]. This technique is considered the fundamental principle of the kinetic theory, which forms the mathematical framework for describing the behavior of gases, called the Maxwell–Boltzmann equation [4,5]. The approach proposed by Chapman (1916) and Enskog (1917) provides a more comprehensive solution for transport phenomena [6,7].

There are two major molecular simulation methods that are based on the kinetic theory of gases, namely, MD Simulation [8] and Direct Simulation Monte Carlo (DSMC) [9]. While DSMC is a probabilistic technique based on molecular collisions, MD provides results that are more realistic and accurate [10,11]. However, since all collisions are processed in the MD method, higher computational resources are required [12]. In many frequently used analytical and numerical solutions to flow problems, equations are simplified with some assumptions. Among these assumptions, a continuum medium, slip/no-slip boundary conditions, constant fluid properties, simplified diffusion mechanisms, empirical viscosity models, 2-D approaches, steadiness, Newtonian or inviscid fluid models, and an isothermal medium can be counted [13,14]. In MD, these macro-scale assumptions are unnecessary and, in some cases, even impossible [15]. As computational power increases, MD simulations of gas flow problems interest more scientists [16,17]. Nevertheless, the difficulty of increasing the number of molecules, thus decreasing the Knudsen number (Kn), is still the main obstacle. Therefore, in order to overcome these computational limitations, simulations based on the hard-sphere model are preferred [18,19]. The hard-sphere model is frequently employed in MD simulations for rarefied gas flows because it effectively represents the fundamental features of gas molecules and their interactions in low-density environments [20]. The hard-sphere model describes gas molecules as solid spheres, enabling the computational simulation of molecular movement and collisions efficiently.

The Knudsen number is a critical parameter in MD simulations for describing gas movements. MD simulations provide reliable solutions for both low Knudsen numbers ($Kn < 0.01$, for the continuum approach) and high Knudsen numbers (for nanochannels and rarefied gas). For low Knudsen numbers, gas behavior becomes like continuum flow, where the mean free path of gas molecules is significantly shorter than the actual size of the flow area. Under these conditions, the movement of gas can be well characterized using continuum-based models, such as the Navier–Stokes equations. As the Knudsen number increases, the behavior of gas shifts towards rarefied flow, where the mean free path becomes similar to or greater than the characteristic length scale. MD simulations are more useful than Navier–Stokes equations for compressible flows because they can offer precise insights into the behavior of compressible gaseous continua at the molecular level. Conducting this investigation at the molecular level enables a more thorough comprehension of compressibility, which is essential for accurately capturing the dynamics of compressible flows [21].

In MD simulations, Couette flow and Poiseuille flow are often used to study the flow of fluids at the molecular level [22–27]. In these simulations, the behavior of individual particles in response to external forces such as shear forces and pressure gradients is investigated. Couette flow is a fundamental concept in fluid dynamics that characterizes the motion of a fluid between two parallel plates, where one plate or two plates move at a constant velocity. This flow structure can be defined by the production of shear stress and the creation of velocity gradients within the fluid. Another approach used in solving physical problems, Poiseuille flow is characterized by a pressure difference (ΔP) along the length of a tube, and the flow is driven by this pressure gradient. It refers to the steady, laminar flow of an incompressible fluid through a pipe or tube. When considering the assumption of incompressibility, there is a simple analytical solution to the problem, and this solution has been examined using various methods [28]. Most MD simulations documented in the literature focus on flows induced by an accelerating body force rather than flows induced by pressure [29–32]. These limitations arise from the use of periodic

boundary conditions that cannot create a pressure gradient within the simulation domain. In many studies, new techniques have been developed to imitate flows caused by pressure differences. Lupkowski & Van Swol (1990) positioned two rigid walls at entry and exit points and then exerted external forces upon them [33]. Li et al. (1998) used an imaginary membrane that allows the unidirectional movement of molecules while reflecting molecules entering from the opposite direction with elastic reflection and certain probability [34]. To et al. dealt with periodic entry and exit velocity conditions, where the square velocity difference between molecules entering and exiting the simulation area is kept constant [35].

In the present study, MD simulations of Couette and Poiseuille flows with the addition of wall temperature effects for a monatomic gas were conducted by utilizing a multi-cell hard-sphere method. Combinations of the coupled effects of wall speeds, pressure gradients, and wall temperatures were investigated to better understand the implications of various parameters. Subsonic, transonic, and supersonic speeds in nanochannels were achieved. In order to illustrate Poiseuille flow, we used a density differentiation algorithm that, for the sake of normalization, eliminates the dependency of variation in molecular mass on imposed pressure gradients. This approach also allowed us to avoid the application of a special thermostatic treatment, which was the case for many Poiseuille flow studies in the literature [36–38]. A membrane with a periodic boundary condition was employed, permitting unidirectional movement of molecules while elastically reflecting molecules approaching from the opposite direction with a specific probability. While we used low spacing ratios in the simulations, the results can be extended to rarefied gas flows of similar Knudsen numbers by using proper scaling [39]. The simulations in this study focus on $0.03 < Kn < 0.14$ and $M < 1.7$ for Knudsen and Mach numbers, respectively. Slips on the walls showed significant results along with explicit overall behaviors. MD was successfully used to investigate wall slips, which is important for investigating wide temperature and velocity ranges. Moreover, these simulations generate realistic profiles of flow characteristics depicting intrinsic behavior. The simulations also enable us to examine the unsteady nature of various flows in detail [40]. In this study, the methodology and model are detailed in Section 2. The simulation results are presented in Section 3, and the conclusions are given in Section 4.

2. Methodology and Model

This section outlines the methodology and computational model employed in our MD study. In the first part, the computational model is explained, and in the second part, the selective permeability that creates a pressure gradient is detailed.

2.1. Computational Model

In this study, the MD simulation method was used to process every molecule and molecular interaction. No real collisions are missed, and no fictitious events are imposed. Serving as the computational domain, a 3-dimensional region (box) was filled with molecules of a compressible fluid, as shown in Figure 1. The monatomic gas molecules are modelled as hard spheres undergoing elastic intermolecular collisions. L_y is a characteristic length in the problem in the y-direction. A molecule–wall interaction model called diffuse reflection is used so that any molecule reaching $\pm y$ walls is reflected back to the computational region with a velocity generated based on the wall characteristics, namely, temperature and velocity [14].

In the z-direction, a complete periodicity condition is applied in which any molecule that reaches a boundary in that direction is instantly transferred to the other boundary, retaining its original velocity. These periodic boundary conditions in the z direction allow for simulations of systems that extend infinitely along the z-axis, providing a more accurate representation of particle behavior without the need for an excessively large simulation box. This is particularly useful in studying systems with periodic or long-range effects, allowing researchers to observe behavior over an extended spatial domain without the computational burden of simulating an infinitely large system. Although there are 2D

Computational Fluid Dynamics (CFD) solutions abounded in the literature when it comes to MD simulations this simplification cannot be applied simply because reducing molecular degree of freedom changes behavior of the gas (for example, speed of sound, heat capacity, specific heat ratios, viscosity, etc.). An algorithm is used for this periodicity condition, which prevents the violation of the primary principle of Event-Driven MD Simulations, which stipulates that any two molecules cannot overlap at any time during the simulation.

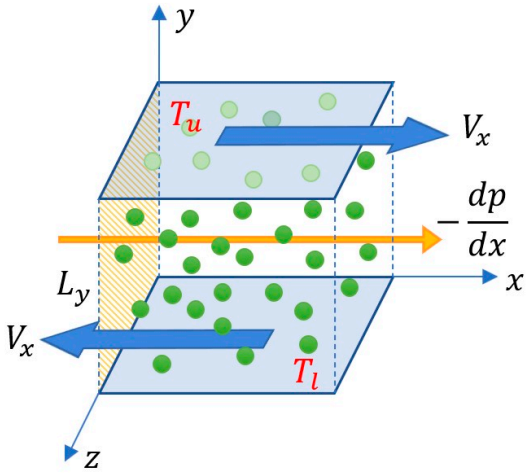

Figure 1. The computational domain used in the simulation.

In order to increase computational speed, the multi-Cell Method is used [41]. In this approach, the whole computational region is divided into cells. This cell division improves computational speed simply because distant molecules are less likely to collide with each other. Nevertheless, molecules can cross multiple cells in 3-dimensional space, and any distant pair of molecules can still interact; no real collision is lost. Any molecule may undergo three major kinds of events: intermolecular collision, cell switching (a pseudo-event), and an outer boundary event (as explained above). Intermolecular collisions cause changes in the velocity components of the colliding pair based on their incoming velocities, masses, sizes, and relative positions through momentum and energy conservation with the assumption of perfectly elastic interaction. Cell switching, as a virtual event, does not really affect the velocity or computational position of a molecule. It merely changes the cell the molecule is assigned to, allowing a new set of molecules in the cellular neighborhood to gain candidacy for becoming a future partner of an interaction. Every molecule has a time variable that is updated after each real event it is involved in while relocating, but this is not the case in cell switching. This approach greatly reduces the incremental errors caused by molecular relocations.

The simulation starts with equally spaced molecules with the same *rms* speeds but arbitrarily different velocity components. The earliest event is calculated and carried out, and then the simulation moves on to the next event. This process repeats in order to generate the simulation. It is worth noting that in a few collisions per particle (cpp), the overall molecular behavior spontaneously adjusts itself to the Maxwellian speed distribution. The whole process is event-driven, and any molecule's position changes only when it is involved in a real event [42–44]. Molecular positions and velocities are the variables defining flow properties such as density, energy, temperature, velocity, pressure, etc. These properties are computed based on the data reduced during the whole simulation using the long-time averaging technique. Despite the computational cost, the time averaging method is used for the sake of accuracy [45]. Instead of using the real, dimensional properties of a gas, non-dimensional input properties are used. All lengths, masses, and speeds are scaled with the molecular diameter of $d = 1$, the molecular mass of $m = 1$, and the *rms* speed of $c_{rms} = \sqrt{15}$, respectively. The last two choices result in a most probable speed of $c_{mp} = \sqrt{10}$ (for which the speed of sound becomes 2.89) and an average initial translational

kinetic energy of $E_x = E_y = E_z = 5$ in any direction. In this study, the molecular spacing ratio is set as $s/d = 3.5$. It is studied in a dimensionless form so that it is applicable to all noble gases, no matter which gas is chosen.

Upper and lower walls ($\pm y$) move in opposite directions at predefined speeds ($\pm V_x$), enabling Couette flow simulations. The lower wall is held at an initial medium temperature ($T_l = 10$), while the upper wall temperature (T_u) is kept at various values ranging from cold to very hot in different simulations. This set of wall temperatures enabled us to examine the effects of different temperature gradients perpendicular to the flow direction. These conditions were fostered by using a modified diffuse reemission algorithm [46,47]. Regardless of the incoming molecular velocity components, reflecting molecular velocity was computed based on these wall conditions by choosing from normal and tangential distributions of the corresponding medium.

2.2. Pressure Gradient

Periodic boundary conditions are frequently employed in MD simulations to represent systems of effectively limitless size by computationally simulating only certain portions of a system. They serve as a fundamental framework for investigating systems in equilibrium, simulating molecular flows under different circumstances and accurately modelling bulk systems by eliminating boundary effects. Periodic boundary conditions have been used to generate flow using an imaginary membrane that allows molecules to pass from one direction and forces molecules coming from the other direction to reflect elastically with a certain probability. In this study, as the third boundary condition, the density difference between upstream and downstream is applied. The probability of passing from the periodic downstream to the upstream boundary is kept at 1, while in the opposite direction, the probability (PW) varies. Note that for $PW = 1.0$, no apparent pressure gradient is expected, and as PW decreases, the gradient becomes stronger.

In this study, a model for a special boundary condition was developed, representing a density variation between the outmost boundaries in the x-direction. The model applies a selective periodicity condition so that the possibility of transferring molecules from the $+x$ boundary to the $-x$ boundary is maintained at a higher level than its counterpart. This is achieved by assigning different probabilities to opposite boundaries' permeabilities and developing an acceptance–rejection algorithm. While all the molecules approaching the $+x$ wall are transferred to the other side, this algorithm is applied to the molecules approaching the $-x$ wall, and this membrane is emphasized by the shaded area in Figure 1. Note that this achieved density variation also generates a pressure gradient in the x-direction.

3. Simulation Results

For combined heat conduction, Couette flow, and simple pressure gradient channel flow, the values given in Table 1 were used. During the simulations, different wall speeds, wall temperatures, and pressure gradients were examined. All the values used are dimensionless. The V_x value, which expresses the wall speed, varies between the value at which the wall has no speed ($V_x = 0.0$) and the value at which the wall speed is $V_x = 5.0$. The speed of sound Is calculated as 2.89, and therefore $V_x = 5.0$ can be considered to be approximately 1.7 Mach. The pressure gradient varies between 1.0 and 0.5. There is no pressure gradient in the case wherein $PW = 1.0$. In the case of $PW = 0.5$, the pressure gradient is at its maximum point, and this means that half of the molecules approaching the wall are reflected to the other side, and the other half are reflected via specular reflection. T_u, which expresses the upper wall temperature, was chosen to be between 4.0 and 22.0, and the lower wall temperature was set as $T_l = 10$ and kept constant in all the simulations.

Table 1. Simulation parameters.

Parameters	**Values**						
V_x	0.0	1.0	2.0	3.0	4.0	5.0	
PW	1.0	0.9	0.8	0.7	0.6	0.5	
T_u	4.0	7.0	10.0	13.0	16.0	19.0	22.0

The simulations were conducted for a set of various numbers of molecules (N) and aspect ratios (AR), as presented in Table 2. The different wall speeds, wall temperatures, and pressure gradients given in Table 1 were applied to these data sets.

Table 2. The data sets.

	Sets of Values				
Parameters	**Set 1**	**Set 2**	**Set 3**	**Set 4**	**Set 5**
AR	1.0	2.0	2.0	4.0	4.0
N	204,800	25,600	51,200	204,800	51,200
Kn	0.0345	0.0689	0.1378	0.0345	0.0689
L_y/d	280	140	70	280	140

In order to converge toward the steady state profiles, a final long-time averaging procedure was computed between 198 and 200 cpp. It was verified that the steady-state conditions were well established by comparing these data with previous cpp values. The local temperature depends on local molecular velocities:

$$3kT \equiv \langle m|\vec{c} - \vec{u}|^2\rangle = m\langle|\vec{c} - \vec{u}|^2\rangle \tag{1}$$

where $\langle\ \rangle$ is an averaging operator, k is the Boltzmann constant, T is absolute temperature, m is molecular mass, $\vec{c}$ is molecular velocity, and $\vec{u}$ is the local velocity vector averaged over the molecules in the vicinity. In our problem, since there are only pressure gradient and velocity boundary conditions acting in the x-direction, we expected a non-zero velocity component only in the x-direction:

$$\langle c_x\rangle = |\vec{u}| = V_x. \tag{2}$$

Substituting Equation (2) into Equation (1) yields

$$3kT = m\langle|\vec{c} - \vec{u}|^2\rangle = m(\langle c^2\rangle - V_x^2). \tag{3}$$

Kinetic energy, on the other hand, is defined as

$$E \equiv \frac{1}{2}mc^2. \tag{4}$$

By using Equations (3) and (4), for temperature, the relationship

$$3kT = 2\langle E\rangle - \langle m\rangle V_x^2 \tag{5}$$

can be deduced.

n denotes number density; pressure is expressed by the state equation:

$$p = nkT \tag{6}$$

As an example, number density plots for when $V_x = 0.0$, $AR = 1.0$, and N = 204,800 are presented in Figure 2. A single simulation took 20 h on a Xeon Power Station HP-Z840 in a single processor run. The first column consisted of zero pressure gradient cases

($PW = 1.0$). In this case, a periodic boundary condition was applied, wherein all molecules approaching the wall pass to the other side. The lower wall was maintained at an initial medium temperature ($T_l = 10$), while the upper wall temperature (T_u) was kept at various values during the simulations. Since $T_u = 10$ corresponds to the same wall temperatures for the upper and lower walls, the third-row, first-column plot represents a case where only the wall velocities are in effect.

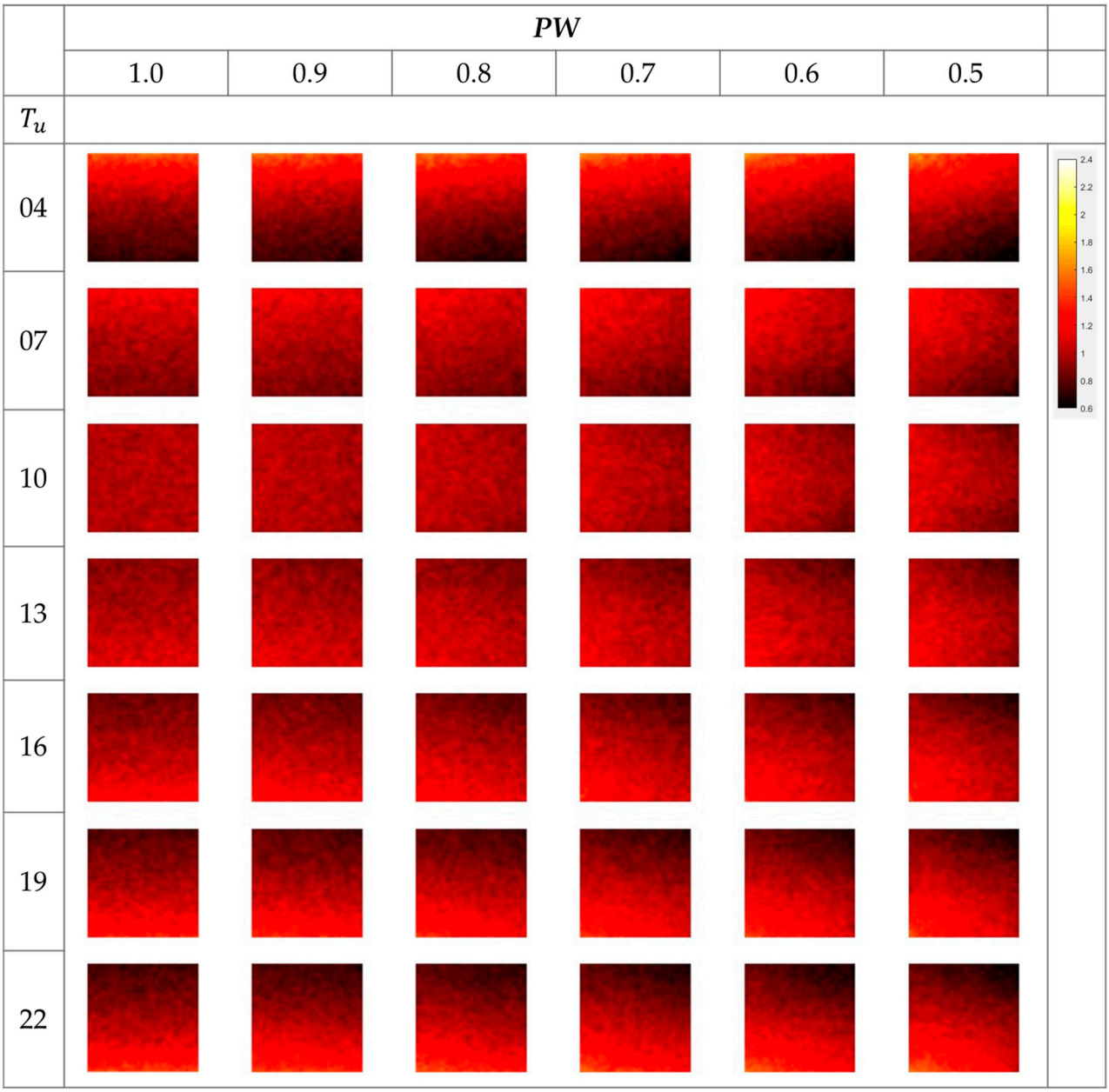

Figure 2. The number density plots for when $V_x = 0.0$, $AR = 1.0$, and N = 204,800.

Figure 3 shows the density plots for when $V_x = 5.0$, $AR = 1.0$, and N = 204,800. In Figures 2 and 3, the first column only shows the effects of velocities and upper-wall temperatures. As the upper wall cools, the number of molecules close to the wall decreases. When $T_u = 4$, the upper wall is considerably colder than the lower wall. The number of molecules increases in the cooling region. This result is clearly depicted in Figure 3, where the speed of the upper wall is high. In the case of $PW = 1.0$, there is no pressure gradient; therefore, the molecules are distributed more homogeneously than when there is a pressure gradient. As the pressure gradient grew stronger, molecules concentrated near

the cold wall. When $T_u = 10$, the lower wall and upper wall temperatures were equal, and the graph is symmetrical in the case where there is no pressure gradient. The 2-D density plots presented in Figures 2 and 3 show variations that agree with the corresponding temperature profiles. Density increases near the cold wall and decreases near the hot wall. The asymmetry of higher-density regions around the corners of cooler walls is caused by the pressure gradient that supports the movement of walls in the forward direction. This is particularly important for the column located on the rightmost side, which has the most intense pressure gradient.

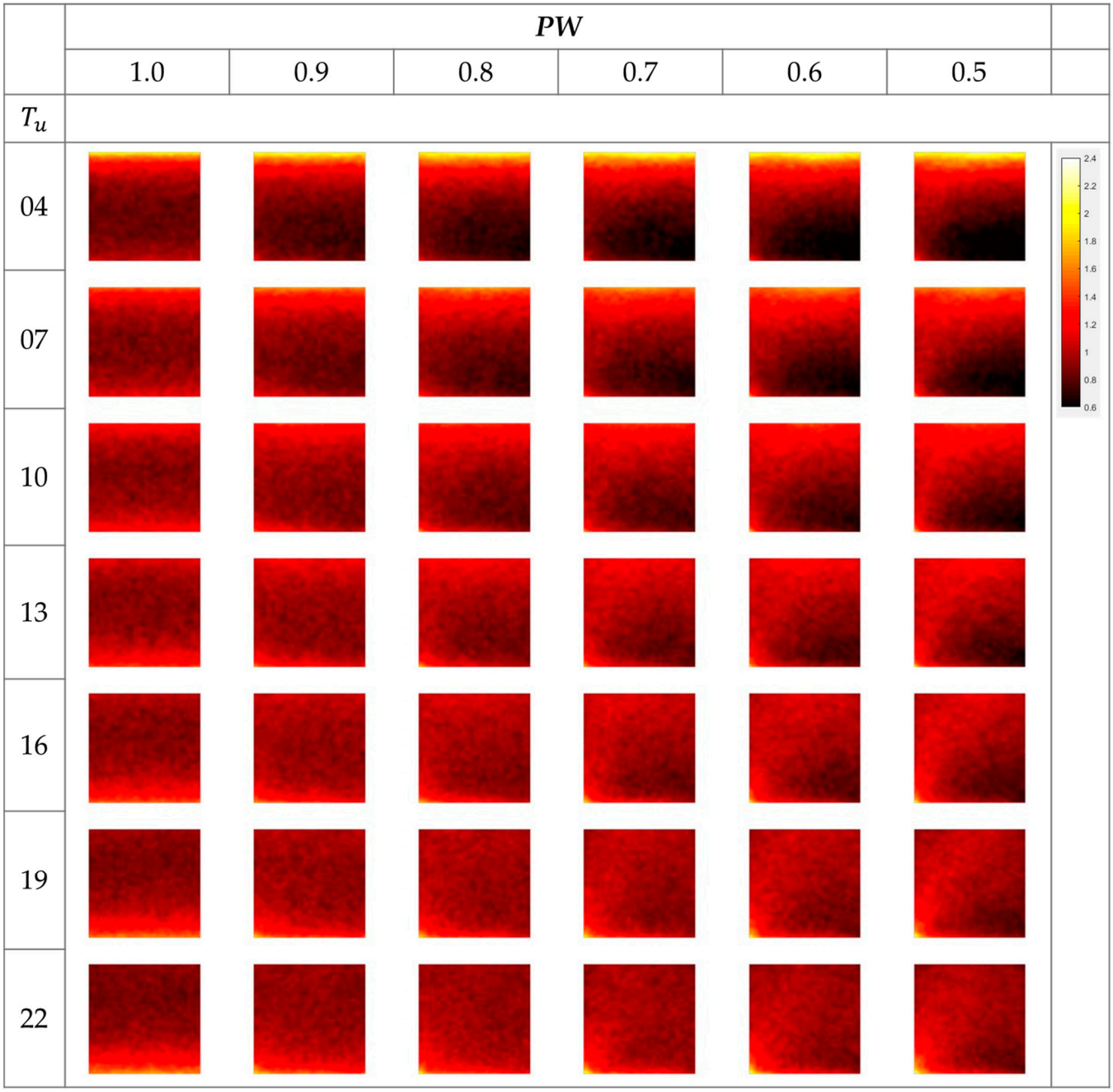

Figure 3. The number density plots for when $V_x = 5.0$, $AR = 1.0$, and N = 204,800.

The pressure difference was considered in the simulation results to examine how the system responded to the pressure difference when a selectively permeable periodic boundary condition was applied. It was observed that the pressure gradients in all the

simulations in this study could be divided into five selected intervals, whose value ranges were taken as approximate values. Table 3 presents these observed pressure gradients. The range with the lowest pressure difference is called dPdx1, and the range with the highest-pressure gradient is called dPdx5.

Table 3. Nomenclature of pressure gradient intervals.

Assigned Name of Pressure Gradient	Corresponding Interval
dPdx1	$-\frac{dP}{dx} < 0.0008$
dPdx2	$0.0020 > -\frac{dP}{dx} > 0.0008$
dPdx3	$0.0032 > -\frac{dP}{dx} > 0.0020$
dPdx4	$0.0043 > -\frac{dP}{dx} > 0.0032$
dPdx5	$-\frac{dP}{dx} > 0.0043$

In Figure 4a–c, variations in average pressure in the computational domain with T_u are depicted for various pairs of wall velocities. A legend corresponding to the dPdx values and wall speeds is given in Figure 4d. Seemingly, in compliance with Equation (6), the average pressure increases almost linearly with T_u. Note that T_u affects the average temperature in the whole region. This behavior is also affected by Couette flow wall velocities simply because faster-moving walls impart more energy to the system, causing a pressure increase. There are bands of velocity ranges arising from the existence of separate cases with different values of Knudsen numbers and aspect ratios.

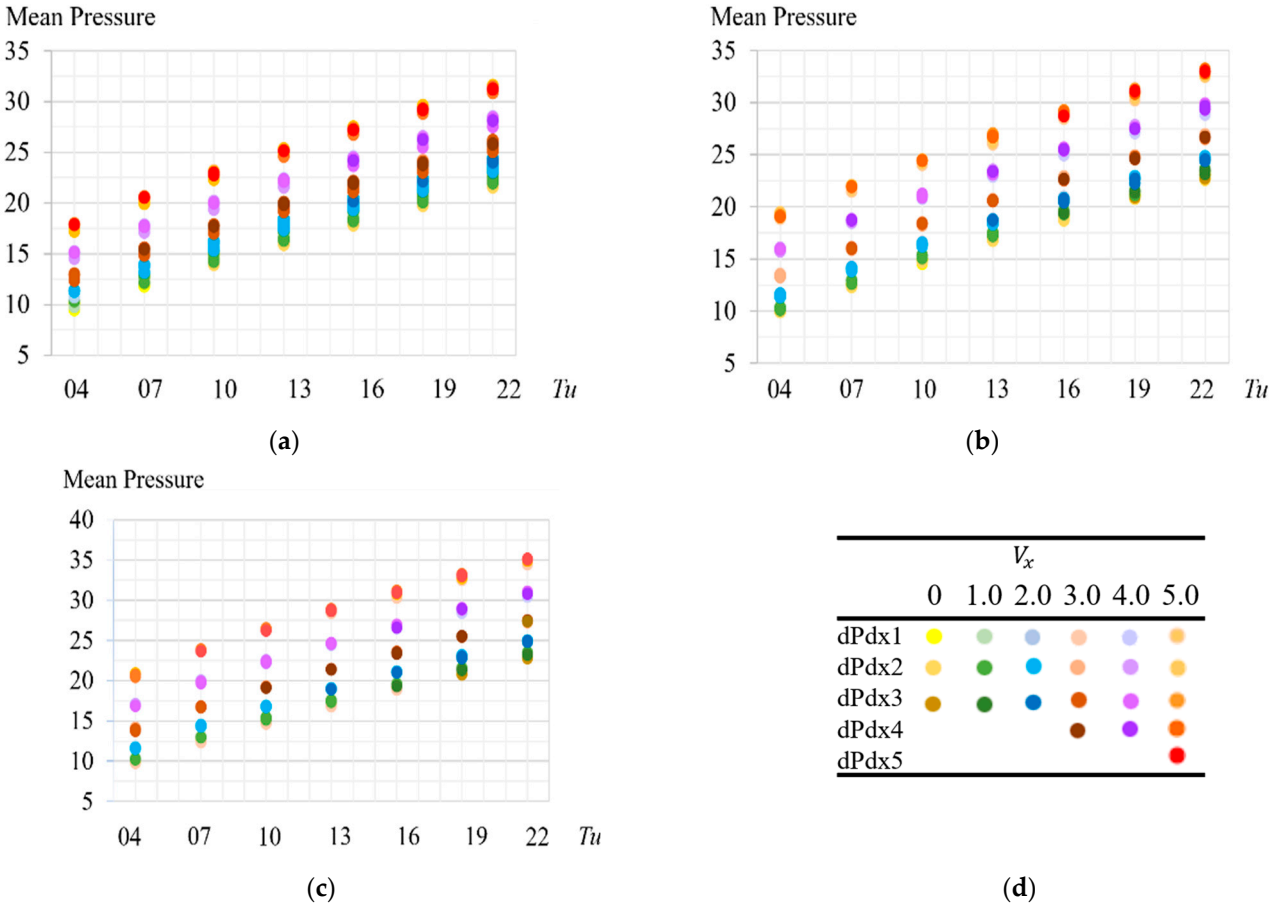

Figure 4. The average pressures in the computational domain for different Kn values: (**a**) $Kn = 0.034$; (**b**) $Kn = 0.069$; (**c**) $Kn = 0.137$; and (**d**) legend.

In Figure 5, the behavior of the relationship between pressure and upper wall temperature is further examined by means of linearly curve fitting the data presented in Figure 4a–c in terms of their Knudsen numbers. In this figure, the effect of Knudsen number and wall velocities on the average pressure is depicted. As the Knudsen number or wall velocities increased, the average pressure increased.

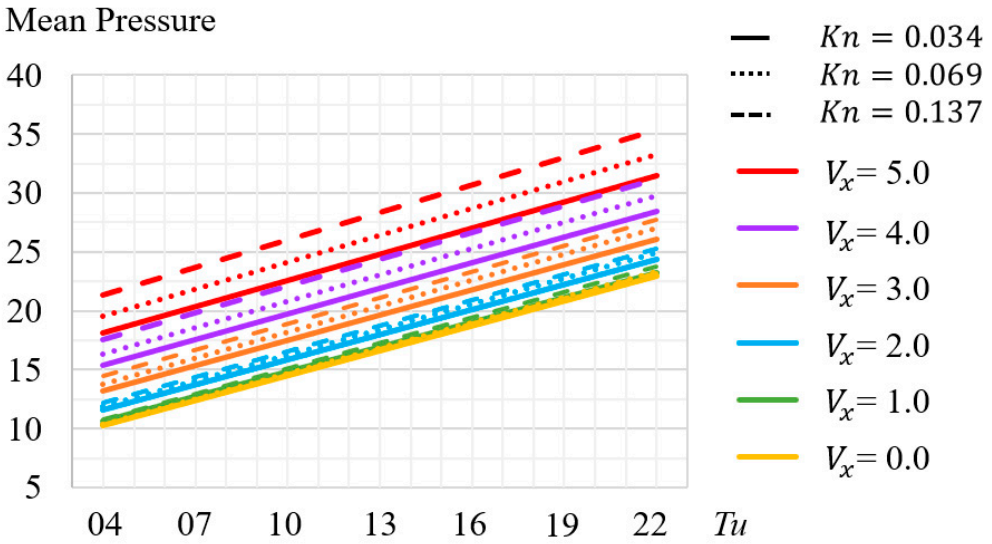

Figure 5. The average pressure in the computational domain for various *Kn* numbers and Couette velocities.

As shown in Figure 5, wall velocity and wall temperature have a linear effect on the average pressure. This linearity is directly affected when the pressure gradient is included in the system. The velocity profiles when $AR = 1.0$ and $N = 204{,}800$ are given in Figure 6. In the first column, the velocity profiles are almost linear because the Knudsen number is low ($Kn = 0.034$) and there is a periodic boundary condition with $PW = 1.0$. As the pressure gradient increases, the nonlinearity in the velocity profiles gains significance. The effect of the pressure gradient on the velocity profiles is greater than that of wall temperature. Note that the velocity slips on the walls are not symmetrical when a pressure gradient exists. For example, in the extreme case when $PW = 0.5$, the velocity slip is greater on the lower wall. The effect of the wall temperatures on the velocity slips seems to be insignificant.

The upper and lower walls move in opposite directions with given velocities. This is why, as per Equation (5), we expected higher temperatures in the middle region. This corresponds to a lower density in the same region because of Equation (6), which is clearly depicted in the plot. This parabolic velocity profile and corresponding temperature profile are shown in Figures 6 and 7, respectively. In Figures 6 and 7, due to the pressure gradient supporting forward-moving walls, the behaviors of higher-density regions accumulated near the corners of colder walls are not symmetrical. This is especially significant for the rightmost column with the strongest pressure gradient.

In Figure 7, the temperature profiles when $AR = 1.0$ and $N = 204{,}800$ are given. When $T_u = 10$, the lower wall and upper wall temperatures are equal, and the graph is symmetrical in the case where $PW = 1.0$. For $T_u \neq T_l$, the profiles are not symmetrical. This figure shows that the temperature slips increase with the increasing wall velocities. Pressure gradients affect these slips as well. Stronger pressure gradients cause greater temperature slips on the lower walls. This is due to the fact that because of the higher pressure at the left wall, some of the molecules traveling upstream are reflected back, while the others are instantly beamed to the right wall with their existing velocity.

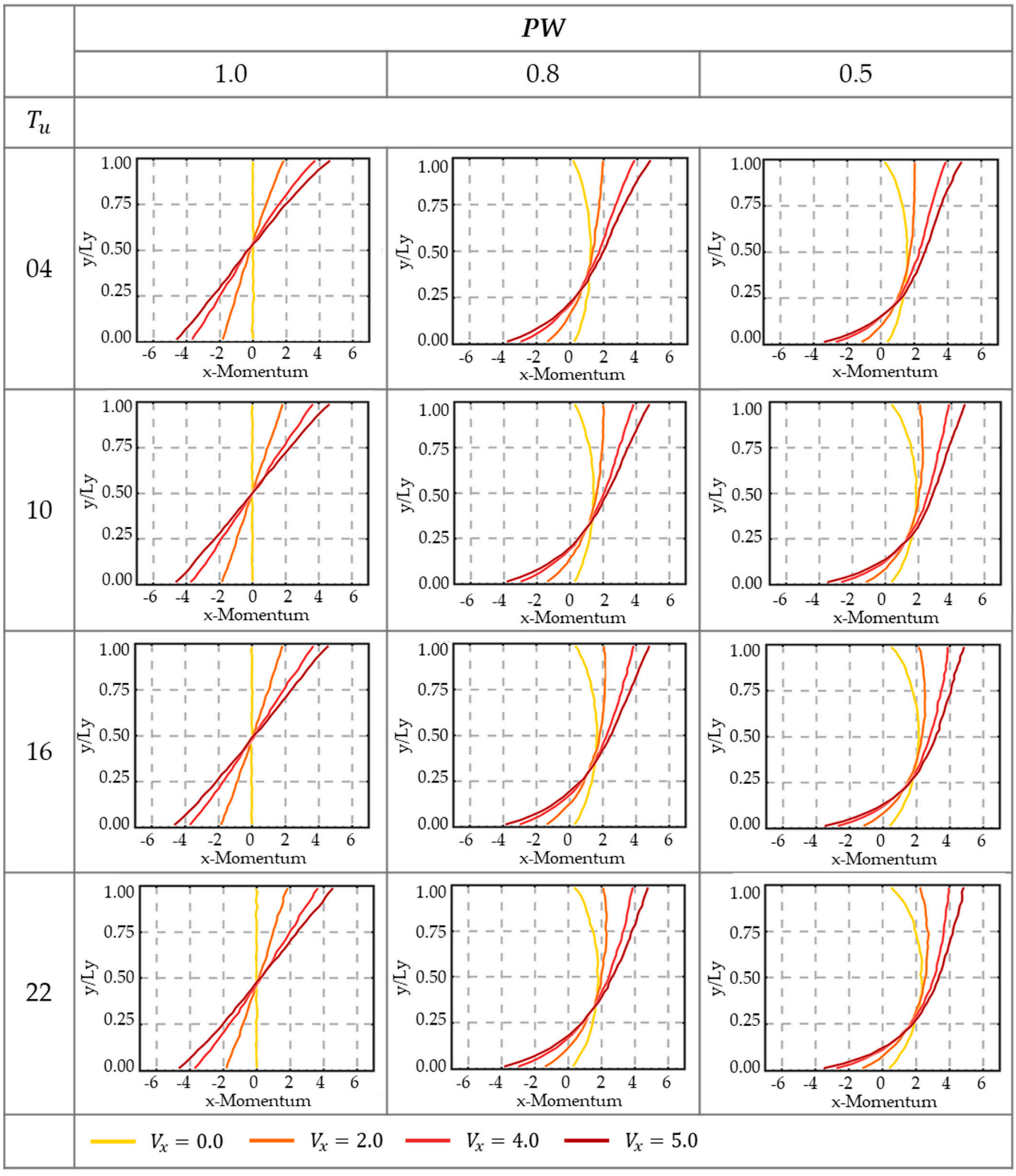

Figure 6. The velocity profiles when $AR = 1.0$ and $N = 204{,}800$.

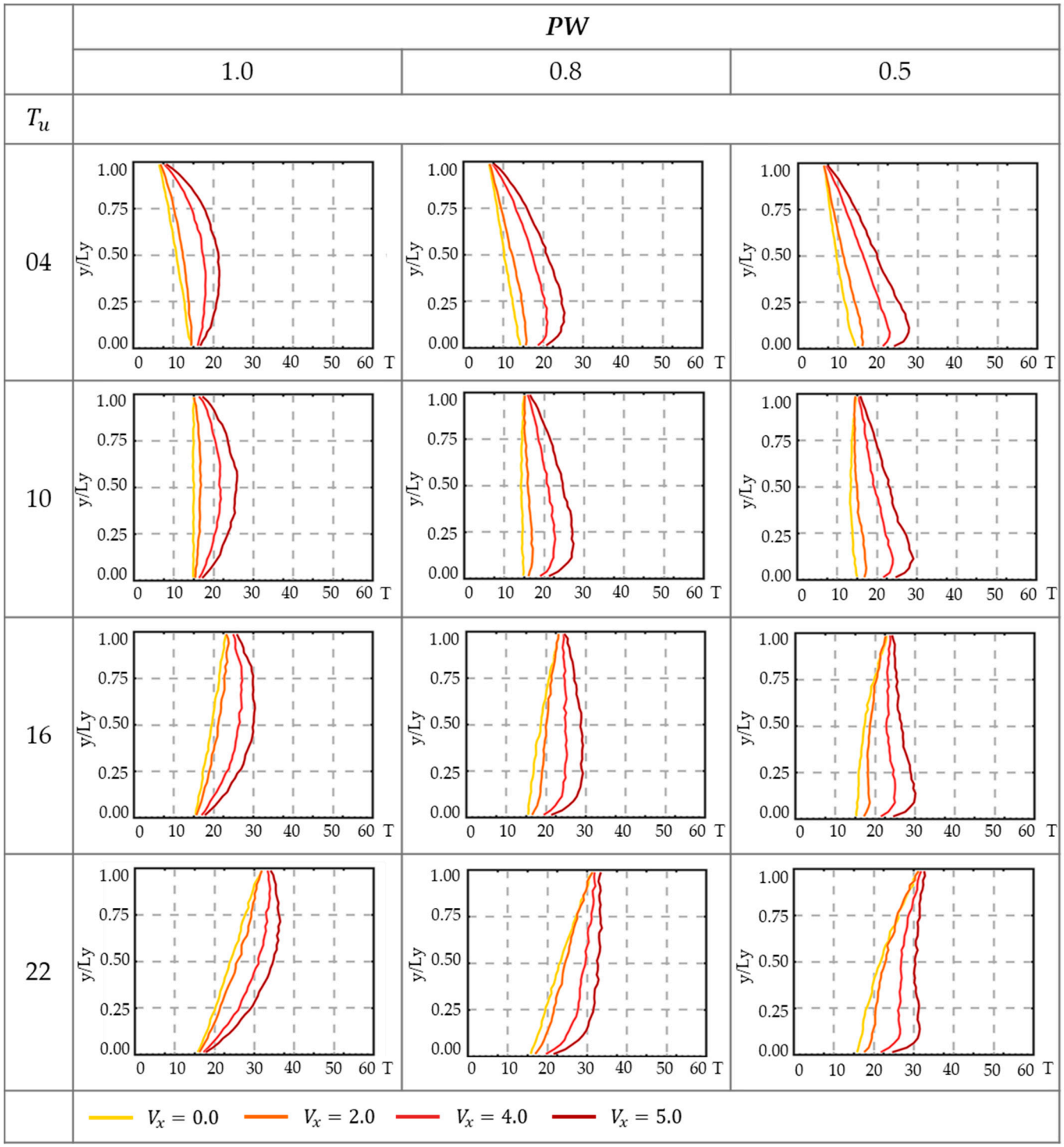

Figure 7. The temperature profiles when $AR = 1.0$ and N = 204,800.

In Figures 6 and 7, the upper and lower walls move in opposite directions at the specified velocities. Therefore, according to Equation (5), we anticipated higher temperatures in the central area. In the temperature profile, a parabolic behavior can be observed because the flow in the middle region is slower, as shown in Figure 6. This behavior identically matches the low-Knudsen-number analytical solution [48]. As PW decreases and, correspondingly, the pressure gradient increases, the profiles in the right column of Figure 7 lose their parabolic nature: a stronger pressure gradient causes a lower peak temperature in the profile. Note that wall velocities strongly define the behavior of the velocity profile near the

walls. The existence of a pressure gradient causes higher velocities around the centerline, as predicted by Poiseuille flow theory. Combined effects of pressure gradient, wall velocities, and temperatures govern different nonlinear temperature and velocity profiles. All these effects cause density variation that plays a role in the region as well.

At the points where the velocity profile becomes zero, the temperature profile achieves a maximum satisfying Equation (5). This behavior is much more intense for supersonic flows.

4. Discussion

In this study, MD simulations of Couette and Poiseuille flows with the addition of wall-temperature effects for a monatomic gas were conducted by using a multi-cell hard-sphere method. Simulations of various parameters, combinations of the coupled effects of wall speeds, pressure gradients, and wall temperatures were executed. Subsonic, transonic, and supersonic speeds in nanochannels are achieved. The periodicity boundary condition in the streamwise direction was modified by developing an acceptance–rejection scheme so that a density difference between upstream and downstream regions formed and yielded a pressure-gradient-driven flow.

In total, the results of 1260 simulation cases were evaluated. The temperature and velocity slips show dependencies not only with respect to the temperature and velocity values but also the magnitudes of the pressure gradient. The pressure gradient also causes nonlinearities in the velocity profiles, which is in compliance with basic flow theory.

In the simulations, the upper and lower walls move in opposite directions at the specified speeds. Therefore, according to Equation (5), we predicted that higher temperatures would occur in the central region. Since the flow in the middle region is slower, a parabolic behavior was observed in the temperature profile. As PW decreases and accordingly the pressure gradient increases, the profiles lose their parabolic properties: a stronger pressure gradient results in a lower peak temperature in the profile. As the pressure gradient becomes stronger, the zero-velocity layer moves toward the wall moving in the opposite direction of the flow.

The molecular spacing ratio in this study is 3.5, which corresponds to a rather high pressure. Additionally, the number of molecules is very low for experimental examination. The application of pressure and temperature gradients complicates the problem of experimental examination even more. Therefore, similar experimental data were not found in the literature. For simple Couette flow, Couette flow with a pressure gradient, and simple Poiseuille flow with a very low Knudsen number ($Kn = 0.034$), our results match the analytical continuum parabolic results for velocity and temperature profiles, which are explained in Figures 6 and 7 in the Simulation Results Section.

It is understood that with the currently available computational capabilities, MD simulations of gases can successfully handle hundreds of thousands of molecules with various combinations of wall temperatures, wall velocities, and pressure gradients in nanochannels of high and low Knudsen numbers.

Author Contributions: E.P.Ö.: Formal analysis, Visualization, Investigation, and Writing; İ.K.: Methodology, Software, Visualization, Writing, and Review and Editing. All authors have read and agreed to the published version of the manuscript.

Funding: This research received no external funding.

Institutional Review Board Statement: Not applicable.

Data Availability Statement: Data are contained within the article.

Acknowledgments: The authors thank TUSAS Engine Industries Inc. (TEI) for granting access to the computational resources developed at Gebze Technical University High-Performance Computing Laboratory.

Conflicts of Interest: The authors declare no conflicts of interest.

References

1. Gad-el-Hak, M. *The MEMS Handbook*; CRC Press: Boca Raton, FL, USA, 2001; Volume 23, ISBN 1420050907.
2. Maxwell, J.C. On the Dynamical Theory of Gases. *Philos. Trans. R. Soc. Lond.* **1867**, *157*, 49–88.
3. Knudsen, M.; Partington, J.R. The Kinetic Theory of Gases: Some Modern Aspects. *J. Phys. Chem.* **1934**, *39*, 307. [CrossRef]
4. Boltzmann, L. Further Studies on the Thermal Equilibrium of Gas Molecules. In Proceedings of the Sitzungsberichte der Akademie der Wissenschaften, Vienna, Austria, 10 October 1872; Volume 66, Part II, pp. 275–370.
5. Maxwell, J.C.; Harmon, P.M. (Eds.) *The Scientific Letters and Papers of James Clerk Maxwell*; Cambridge University Press: Cambridge, UK, 1995; Volume II, pp. 1862–1873.
6. Chapman, S. The Kinetic Theory of Simple and Composite Monatomic Gases: Viscosity, Thermal Conduction, and Diffusion. *Proc. R. Soc. Lond. Ser. A* **1916**, *93*, 1–20. [CrossRef]
7. Enskog, D. *Kinetische Theorie der Vorgänge in Mässig Verdünnten Gasen*; Almquist & Wiksell: Uppsala, Sweden, 1917; Volume 1.
8. JAlder, B.J.; Wainwright, T.E. Phase Transition for a Hard Sphere System. *J. Chem. Phys.* **1957**, *27*, 1208–1209. [CrossRef]
9. Bird, G.A. *Molecular Gas Dynamics and the Direct Simulation of Gas Flows*; Oxford University Press: Oxford, UK, 1994.
10. Han, Y.L.; Muntz, E.P.; Alexeenko, A.; Young, M. Experimental and Computational Studies of Temperature Gradient-Driven Molecular Transport in Gas Flows through Nano/Microscale Channels. *Nanoscale Microscale Thermophys. Eng.* **2007**, *11*, 151–175. [CrossRef]
11. Tohidi, M.; Toghraie, D. The Effect of Geometrical Parameters, Roughness and the Number of Nanoparticles on the Self-Diffusion Coefficient in Couette Flow in a Nanochannel by Using of Molecular Dynamics Simulation. *Phys. B Condens. Matter* **2017**, *518*, 20–32. [CrossRef]
12. Haile, J.M. *Molecular Dynamics Simulation: Elementary Methods*; Wiley: Chichester, UK, 1992; ISBN 0-471-81966-2.
13. Duck, P.W.; Erlebacher, G.; Hussaini, M.Y. On the Linear Stability of Compressible Plane Couette Flow. *J. Fluid Mech.* **1994**, *258*, 131–165. [CrossRef]
14. Bird, G.A. Molecular Gas Dynamics. *NASA STI/Recon Tech. Rep. A* **1976**, *76*, 40225.
15. Gad-el-Hak, M. Liquids: The Holy Grail of Microfluidic Modeling. *Phys. Fluids* **2005**, *17*, 100612. [CrossRef]
16. Abramov, A.A.; Butkovskii, A.V. Couette Flow Regimes with Heat Transfer in Rarefied Gas. *J. Exp. Theor. Phys.* **2013**, *116*, 1036–1042. [CrossRef]
17. Xie, J. A Mean Free Path Approach to the Micro/Nanochannel Gas Flows. *Adv. Aerodyn.* **2020**, *2*, 11. [CrossRef]
18. Akkaya, V.R.; Kandemir, I. Event-Driven Molecular Dynamics Simulation of Hard-Sphere Gas Flows in Microchannels. *Math. Probl. Eng.* **2015**, *2015*, 842837. [CrossRef]
19. Koc, M.; Kandemir, I.; Akkaya, V.R. An Investigation of Transition Flow in Porous Media by Event Driven Molecular Dynamics Simulation. *J. Appl. Fluid Mech.* **2021**, *14*, 23–36. [CrossRef]
20. Rabani, R.; Heidarinejad, G.; Harting, J.; Shirani, E. Heat Conduction Characteristic of Rarefied Gas in Nanochannel. *J. Appl. Fluid Mech.* **2020**, *13*, 1–13. [CrossRef]
21. Xiao, H.; He, Q.J.; Xiao, X.; Lian, Y.D. Molecular-Level Study of Compressible Gaseous Continua. *J. Phys. Commun.* **2018**, *2*, 095006. [CrossRef]
22. Zahid, W.A.; Yin, Y.; Zhu, K.Q. Couette-Poiseuille Flow of a Gas in Long Microchannels. *Microfluid. Nanofluidics* **2007**, *3*, 55–64. [CrossRef]
23. Ali, A.O.; Makinde, O.D. Modelling the Effect of Variable Viscosity on Unsteady Couette Flow of Nanofluids with Convective Cooling. *J. Appl. Fluid Mech.* **2015**, *8*, 793–802. [CrossRef]
24. Assadi, S.; Kalteh, M.; Bagheri Motlagh, M. Investigating Convective Heat Transfer Coefficient of Nanofluid Couette Flow in a Nanochannel by Molecular Dynamics Simulation. *Mol. Simul.* **2022**, *48*, 702–711. [CrossRef]
25. Ziarani, A.S.; Mohamad, A.A. A Molecular Dynamics Study of Perturbed Poiseuille Flow in a Nanochannel. *Microfluid. Nanofluidics* **2006**, *2*, 12–20. [CrossRef]
26. Ebrahimi, A.; Shahabi, V.; Roohi, E. Pressure-Driven Nitrogen Flow in Divergent Microchannels with Isothermal Walls. *Appl. Sci.* **2021**, *11*, 3602. [CrossRef]
27. Kannan, A.S.; Narahari, T.S.B.; Bharadhwaj, Y.; Mark, A.; Sardina, G.; Maggiolo, D.; Sasic, S.; Ström, H. The Knudsen Paradox in Micro-Channel Poiseuille Flows with a Symmetric Particle. *Appl. Sci.* **2021**, *11*, 351. [CrossRef]
28. Karniadakis, G.E.; Beskok, A.; Aluru, N.R. Microflows and Nanoflows Fundamentals and Simulation. In *Interdisciplinary Applied Mathematics*; Springer: Berlin/Heidelberg, Germany, 2005; Volume 29, pp. 1–61.
29. Todd, B.D.; Evans, D.J. Temperature Profile for Poiseuille Flow. *Phys. Rev. E Stat. Phys. Plasmas Fluids Relat. Interdiscip. Top.* **1997**, *55*, 2800–2807. [CrossRef]
30. Bhattacharya, D.K.; Lie, G.C. Molecular-Dynamics Simulations of Nonequilibrium Heat and Momentum Transport in Very Dilute Gases. *Phys. Rev. Lett.* **1989**, *62*, 897–900. [CrossRef] [PubMed]
31. To, Q.D.; Bercegeay, C.; Lauriat, G.; Léonard, C.; Bonnet, G. A Slip Model for Micro/Nano Gas Flows Induced by Body Forces. *Microfluid. Nanofluidics* **2010**, *8*, 417–422. [CrossRef]
32. Barrat, J.L.; Bocquet, L. Large Slip Effect at a Nonwetting Fluid-Solid Interface. *Phys. Rev. Lett.* **1999**, *82*, 4671. [CrossRef]
33. Lupkowski, M.; Van Swol, F. Computer Simulation of Fluids Interacting with Fluctuating Walls. *J. Chem. Phys.* **1990**, *93*, 737–745. [CrossRef]

34. Li, J.; Liao, D.; Yip, S. Coupling Continuum to Molecular-Dynamics Simulation: Reflecting Particle Method and the Field Estimator. *Phys. Rev. E* **1998**, *57*, 7259–7267. [CrossRef]
35. To, Q.D.; Pham, T.T.; Lauriat, G.; Léonard, C. Molecular Dynamics Simulations of Pressure-Driven Flows and Comparison with Acceleration-Driven Flows. *Adv. Mech. Eng.* **2012**, *4*, 580763. [CrossRef]
36. Cao, B.Y.; Chen, M.; Guo, Z.Y. Effect of Surface Roughness on Gas Flow in Microchannels by Molecular Dynamics Simulation. *Int. J. Eng. Sci.* **2006**, *44*, 927–937. [CrossRef]
37. Guo, Y.; Surblys, D.; Kawagoe, Y.; Matsubara, H.; Liu, X.; Ohara, T. A Molecular Dynamics Study on the Effect of Surfactant Adsorption on Heat Transfer at a Solid-Liquid Interface. *Int. J. Heat Mass Transf.* **2019**, *135*, 115–123. [CrossRef]
38. Aoki, K.; Sone, Y.; Ohwada, T. Heat Transfer and Temperature Distribution in a Rarefied Gas Between Two Parallel Plates with Different Temperatures: Numerical Analysis of the Boltzmann Equation for a Hard Sphere Molecule. *Rarefied Gas Dyn. Theor. Comput. Tech.* **1989**, *118*, 70–81. [CrossRef]
39. Greber, I.; Wachman, H. Scaling Rules and Time Averaging in Molecular Dynamics Computations of Transport Properties. *Prog. Astronaut. Aeronaut.* **1989**, *117*, 194–207.
40. Risso, D.; Cordero, P. Dilute Gas Couette Flow: Theory and Molecular Dynamics Simulation. *Phys. Rev. E* **1997**, *56*, 7365. [CrossRef]
41. Kandemir, I. A Multicell Molecular Dynamics Method. Ph.D. Thesis, Case Western Reserve University, Cleveland, OH, USA, 1999.
42. Kandemir, I.; Greber, I.; Woo, M. Heat Conduction and Couette Flow in a Hard Sphere Gas Using a Multicell Molecular Dynamics Computational Method. In Proceedings of the 21st International Symposium of Rarefied Gas Dynamics, Marseille, France, 26–31 July 1998; Volume 1, pp. 1–8.
43. Kandemir, I.; Kaya, A.M. Molecular Dynamics Simulation of Compressible Hot/Cold Moving Lid-Driven Microcavity Flow. *Microfluid. Nanofluidics* **2011**, *12*, 509–520. [CrossRef]
44. Smallenburg, F. Efficient Event-Driven Simulations of Hard Spheres. *Eur. Phys. J. E* **2022**, *45*, 22. [CrossRef]
45. Gordiz, K.; Singh, D.J.; Henry, A. Ensemble Averaging vs. Time Averaging in Molecular Dynamics Simulations of Thermal Conductivity. *J. Appl. Phys.* **2015**, *117*, 045104. [CrossRef]
46. Ohwada, T.; Sone, Y.; Aoki, K. Numerical Analysis of the Shear and Thermal Creep Flows of a Rarefied Gas over a Plane Wall on the Basis of the Linearized Boltzmann Equation for Hard-sphere Molecules. *Phys. Fluids A Fluid Dyn.* **1989**, *1*, 1588–1599. [CrossRef]
47. Sone, Y.; Ohwada, T.; Aoki, K. Temperature jump and Knudsen layer in a rarefied gas over a plane wall: Numerical analysis of the linearized Boltzmann equation for hard-sphere molecules. *Phys. Fluids A Fluid Dyn.* **1989**, *1*, 363–370. [CrossRef]
48. Kandemir, I.; Sevilgen, F.E. Molecular Dynamics Simulation of Helium-Argon Gas Mixture under Various Wall Conditions. *Mol. Simul.* **2008**, *34*, 795–808. [CrossRef]